Virology 530 (2019) 19–26

Contents lists available at ScienceDirect

Virology

journal homepage: www.elsevier.com/locate/virology

Mutations present in a low-passage Zika virus isolate result in attenuated pathogenesis in mice

Nisha K. Duggal[a,b,*], Erin M. McDonald[b], James Weger-Lucarelli[a,c], Seth A. Hawks[a], Jana M. Ritter[d], Hannah Romo[b], Gregory D. Ebel[c], Aaron C. Brault[b,**]

[a] Department of Biomedical Sciences and Pathobiology, Virginia Polytechnic Institute and State University, Blacksburg, VA, United States
[b] Division of Vector-borne Diseases, Centers for Disease Control and Prevention, Fort Collins, CO, United States
[c] Department of Microbiology, Immunology, and Pathology, Colorado State University, Fort Collins, CO, United States
[d] Division of High-Consequence Pathogens and Pathology, Centers for Disease Control and Prevention, Atlanta, GA, United States

ARTICLE INFO

Keywords:
Zika virus
Flavivirus
Mouse model
Viral pathogenesis

ABSTRACT

Zika virus (ZIKV) infection can result in neurological disorders including Congenital Zika Syndrome in infants exposed to the virus *in utero*. Pregnant women can be infected by mosquito bite as well as by sexual transmission from infected men. Herein, the variants of ZIKV within the male reproductive tract and ejaculates were assessed in inoculated mice. We identified two non-synonymous variants at positions E-V330L and NS1-W98G. These variants were also present in the passage three PRVABC59 isolate and infectious clone relative to the patient serum PRVABC59 sequence. In subsequent studies, ZIKV E-330L was less pathogenic in mice than ZIKV E-330V as evident by increased average survival times. In Vero cells, ZIKV E-330L/NS1-98G outcompeted ZIKV E-330V/NS1-98W within 3 passages. These results suggest that the E-330L/NS1-98G variants are attenuating in mice and were enriched during cell culture passaging. Cell culture propagation of ZIKV could significantly affect animal model development and vaccine efficacy studies.

1. Introduction

Zika virus (ZIKV; *Flaviviridae*) is a mosquito-borne neurotropic virus that can elicit neurological disease including Guillain-Barré syndrome and congenital disease in fetuses when exposed *in utero*. Congenital pathological manifestations include ocular lesions and brain malformations that have collectively been described as Congenital Zika Syndrome (CGS). ZIKV has been extensively documented to be transmitted sexually, a potential exposure route that has been shown to exacerbate the exposure risk of developing fetuses in mice (Duggal et al., 2018). The neurotropism of ZIKV has been extensively demonstrated in mice and non-human primates, with tropism to additional tissues including the male and female reproductive tract (Lazear et al., 2016; Rossi et al., 2016; Govero et al., 2016; Ma et al., 2016). ZIKV can persist in the male reproductive tract of animals for many weeks after viremia has cleared (Duggal et al., 2017a), suggesting ZIKV has the potential to adapt to the male reproductive tract before sexual transmission. Thus sexually transmitted variants may differ from serum-derived isolates, and some sexually transmitted variants may be more efficiently transmitted, such as with other sexually transmitted viruses including HIV-1 (Joseph et al., 2015).

In animal models, African ZIKV strains have been shown to elicit greater pathogenic effects and viral titers in the brain and male reproductive tract compared to Asian and American strains (McDonald et al., 2017; Smith et al., 2018). While the African isolate MR766 has an extensive passage history in sucking mouse brains that could be associated with increased neurovirulence, the low passage African strain DakAr41524 also has demonstrated increased neurovirulence in intracranially inoculated adult immune competent mice compared to an Asian genotype isolate (Duggal et al., 2017b). Many other ZIKV isolates used in animal models are low-passage and are thought to reflect circulating strains; however, a commonly used American isolate PRVABC59 that has been propagated only three times in Vero cells from the serum of an individual returning from Puerto Rico has multiple non-synonymous variants (Weger-Lucarelli et al., 2017). This isolate has been distributed extensively and has been used for pathogenesis testing in animal models as well as a vaccine challenge strain for vaccine efficacy studies. Variants generated from cell culture passaging may influence these *in vivo* studies.

To assess the adaptation of ZIKV to the male reproductive tract

* Correspondence to: 1981 Kraft Drive, Blacksburg, VA 24061, United States.
** Correspondence to: 3156 Rampart Road, Fort Collins, CO 80521, United States.
E-mail addresses: nduggal@vt.edu (N.K. Duggal), abrault@cdc.gov (A.C. Brault).

https://doi.org/10.1016/j.virol.2019.02.004
Received 7 December 2018; Received in revised form 5 February 2019; Accepted 6 February 2019
Available online 07 February 2019

during sexual transmission and to cell culture during passaging, viral genetic variants were identified in infected male mice and after passaging in Vero cells. Compared to the original patient serum from which the ZIKV strain (PRVABC59) was isolated, two non-synonymous variants at E-330 and NS1–98 were identified at high frequency in the male reproductive tract and ejaculates of inoculated mice, as well as in the Vero passage three virus stock used for inoculation. These mutations were assessed *in vitro* and *in vivo* and were found to alter viral fitness in cell culture and pathogenesis in mice. These studies indicate that these mutations were observed in ZIKV within three cell culture passages, and these mutations may significantly alter pathogenesis in animal models.

2. Results

2.1. ZIKV genetic variants within infected mice

The widely-distributed ZIKV isolate PRVABC59 was derived from serum from an individual in Puerto Rico in 2015 (Lanciotti et al., 2016). The virus was originally deep sequenced directly from patient serum and was then passaged in Vero cells three times. The passage three isolate was distributed extensively for use in research laboratories around the world. Here, deep sequencing was performed on the passage three PRVABC59 isolate, as well as viral RNA extracted from the testes and ejaculates collected from twelve AG129 mice previously inoculated with the passage three PRVABC59 isolate for studies of sexual transmission (Duggal et al., 2017a). Two non-synonymous variants were present in envelope at residue 330 (valine to leucine) and NS1 at residue 98 (tryptophan to glycine) in the passage 3 isolate at 58% and 32% frequencies, respectively (Fig. 1). These variants increased in frequency to 92% and 75%, respectively, in the testes of AG129 mice and increased again to 96% and 88%, respectively, in the ejaculates of these mice (Fig. 1). In contrast, three synonymous variants at NS1–177, NS5–627, and NS5–860 were present in the passage 3 isolate at 15%, 18%, and 22% frequencies, respectively. These variants did not increase in frequency in the testes or ejaculates (Fig. 1). These data suggest that the E-330 and NS1–98 variants may have been adaptive variants during dissemination in the male murine reproductive tract.

Furthermore, the sequencing data from the original patient serum containing PRVABC59 previously generated in (Lanciotti et al., 2016) was investigated for the presence of the E-330L and NS1–98G variants. The E-330L variant was present in the patient serum in 2.6% of reads, and the NS1–98G variant was present in 0.4% of reads (Fig. 1). Together, these data suggest that the E-330L and NS1–98G variants may also have been cell culture adaptive mutations.

2.2. Single E-V330L point mutation decreases ZIKV pathogenesis in immunodeficient mice

To test whether the E-330L and NS1–98G mutations alter pathogenesis of ZIKV in mice, the mutations were reverse engineered into an infectious clone based on PRVABC59 (Weger-Lucarelli et al., 2017). Because of the high frequency of the E-330L mutation in the passage 3 isolate that the infectious clone was derived from, this mutation was present in the original plasmid, and the revertant mutation (E-330V) was engineered. The virus most similar to the patient serum sample is E-330V/NS1-98W. The virus with the single derived E-330 mutation was designated as E-330L/NS1–98W and is the equivalent of the original infectious clone described in (Weger-Lucarelli et al., 2017). A virus with both derived mutations was also generated and designated as E-330L/NS1-98G. To confirm that the E-330L and NS1–98G variants were present in the same genome in the passage three isolate, an RT-PCR amplicon generated from the virus stock was sub-cloned, and the double mutation was identified in multiple clones.

Male AG129 mice were inoculated in groups of 12 with the viruses containing E-330V/NS1-98W, E-330L/NS1–98W, or E-330L/NS1–98G *via* subcutaneous inoculation. Weight loss began on day post-inoculation (dpi) 6, with significant weight loss occurring from dpi 7–9 in the mice inoculated with E-330V/NS1-98W as compared to mice inoculated with the single or double mutant viruses (Fig. 2A, $p < 0.05$). Inoculation with the E-330V/NS1-98W virus also resulted in a significantly shorter median survival time (9 days; $p < 0.05$) compared to the single and double mutant. There were no differences in weight loss or survival time between mice inoculated with the viruses containing the single or double mutation (Fig. 2B, $p = 0.50$).

2.3. The E-V330L mutation decreases ZIKV dissemination in immunodeficient mice

Mice inoculated with the E-330V/NS1-98W virus had significantly higher serum viral titers at dpi 1, 3, and 5 compared to mice inoculated with the E-330L/NS1–98W or E-330L/NS1–98W mutant viruses (Fig. 3). For all three groups, peak viremia occurred on dpi 3. None of the mice had viremia beyond dpi 7.

To determine the kinetics of ZIKV dissemination to tissues, three AG129 mice from each group were euthanized on dpi 6 and dpi 9. The infectious ZIKV titers in brain, eye, seminal vesicles, epididymides and testes were measured by plaque assay. By dpi 9 there were significantly higher viral titers in many tissues, including the testes (Fig. 4A, $p < 0.01$), seminal vesicles (Fig. 4B, $p < 0.01$), eye (Fig. 4D, $p < 0.01$), and brain (Fig. 4E, $p < 0.01$) of the mice inoculated with the E-330V/NS1-98W virus compared to mice inoculated with the E-330L/NS1-98W or E-330L/NS1-98G viruses. On dpi 6, epididymal titers were significantly higher in the mice inoculated with the E-330V/NS1-98W virus compared to the E-330L/NS1-98W virus (Fig. 4C, $p < 0.05$), but not compared to mice inoculated with the E-330L/NS1-98G virus (Fig. 4C, $p = 0.08$). On dpi 9, which is near the peak of sexual transmission efficiency (Fig. 4G), the epididymal titers were not significantly different across groups. Viremia was not significantly different between any group at dpi 6 and was not detectable at dpi 9 (Fig. 4F). Next, in order to test whether the NS1-98G mutation altered sexual transmission efficiency, ejaculates were collected from inoculated mice. Because of the short survival time of mice inoculated with the E-330V/NS1-98W virus, ejaculates were not collected from this group. Ejaculates from mice inoculated with the E-330L/NS1-98W or E-330L/NS1-98G viruses contained infectious ZIKV from dpi 7–14 with no significant difference in titers (Fig. 4G). Ejaculates beyond dpi 14 were only collected for the mice inoculated with the E-330L/NS1-98G mutant, and they contained low levels of ZIKV RNA (Fig. 4H). Thus, the mice inoculated with the E-330L/NS1-98G virus had a sexual transmission efficiency indistinguishable from the mice inoculated with the E-330L/NS1-98W virus. To determine whether the mutations were stable *in vivo*, ZIKV was sequenced from the serum of three mice per group, and the mutations were confirmed at the consensus level (data not shown). These data suggest that the variants are not adaptive to the male reproductive tract.

Histopathology and ZIKV RNA localization by *in situ* hybridization (ISH) were performed on the aforementioned tissues for 3 mice from each group at dpi 9. Overall findings correlated with the viral titer data. Brains from mice inoculated with the E-330V/NS1-98W virus showed patchy, mild to moderate meningeal and parenchymal intravascular leukocytosis and perivascular mixed inflammation, and multifocal neuronal necrosis with parenchymal inflammation. Changes were variably prominent throughout the cerebrum and within the hippocampus, brainstem, and cerebellum. Labeling of ZIKV RNA by ISH was extensive throughout the entire brain (Fig. 5A, left panel). Brains from mice inoculated with the E-330L/NS1-98W virus showed similar, scattered foci of necrosis and inflammation, but to a lesser extent than observed in brains from mice inoculated with E-330V/NS1-98W, and ISH showed correspondingly less staining (Fig. 5A, middle panel). Two of three brains from mice inoculated with E-330L/NS1-98G showed no histopathologic alterations and no viral RNA labeling by ISH. One brain showed scattered labeling by ISH in the olfactory bulb, cerebral nuclei,

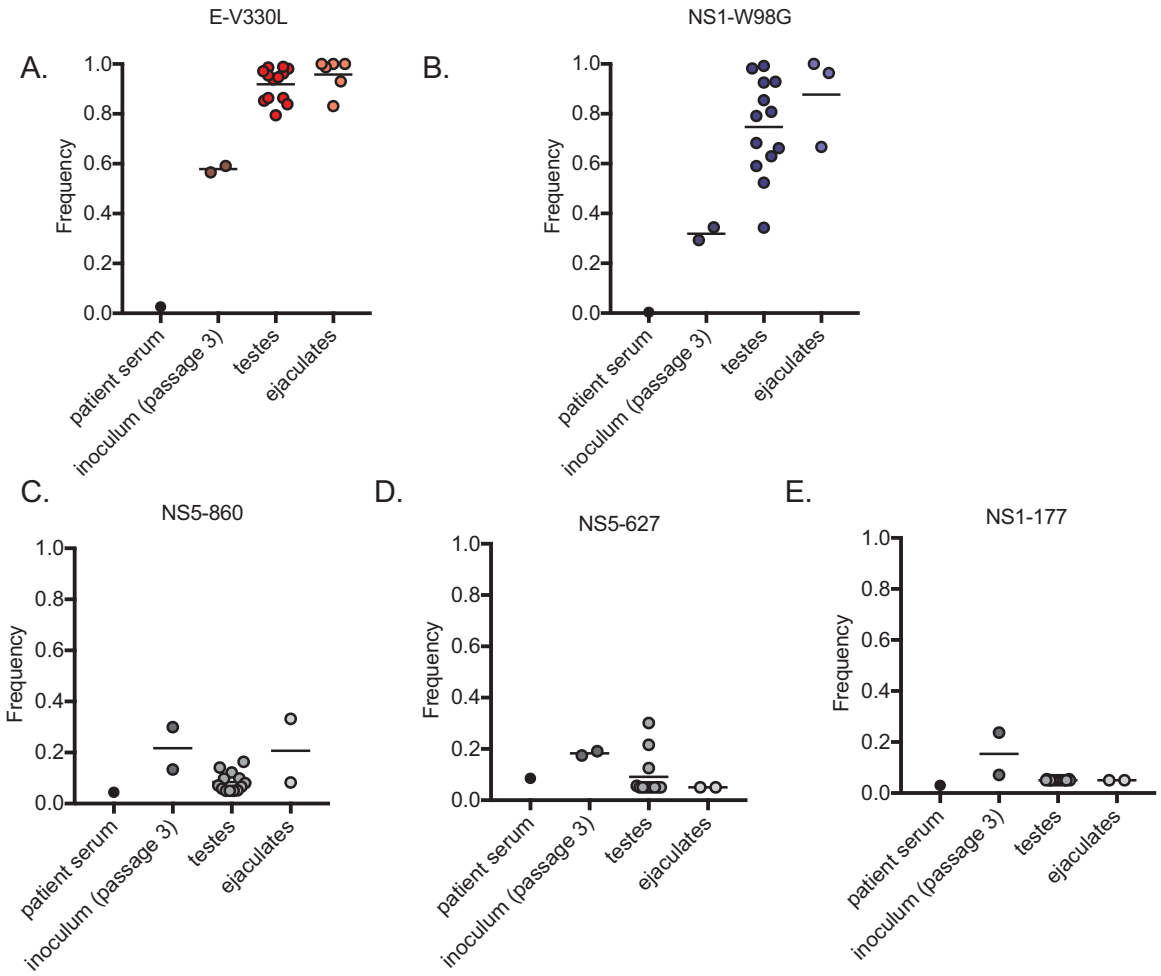

Fig. 1. Increasing frequencies of ZIKV mutations. Frequencies of single nucleotide variants in PRVABC59 sequenced from patient serum, passage 3 virus stocks (inoculum), and in the testes and ejaculates of inoculated AG129 mice (A) E-V330L (B) NS1-W98G (C) NS5-860 (synonymous variant) (D) NS5-627 (synonymous variant) (E) NS1-177 (synonymous variant).

hippocampus, and pons, without overt necrosis or inflammation (Fig. 5A, right panel).

Eye, testis, and seminal vesicle had pathologic changes in mice inoculated with the E-330V/NS1-98W virus only (Fig. 5B). All mice had mild neutrophilic infiltrates and fibrin within the vitreous chamber and inner retina, with associated ZIKV RNA labeling by ISH in the inner retinal layers (Fig. 5B, first panel). Two of three mice had testicular teratomas (Fig. 5B, second panel), and the third mouse had subacute interstitial testicular inflammation and diffuse seminiferous epithelial degeneration (Fig. 5B, third panel). Teratomas showed extensive labeling by ZIKV ISH in neural and epithelial components. The other testis showed scattered labeling within peritubular myoid cells and seminiferous epithelium. Seminal vesicles from 1 of 3 mice had focal mucosal necrosis with ZIKV RNA labeling by ISH (Fig. 5B, fourth panel). The vas deferens had no histopathologic abnormalities and showed no labeling by ISH for any mouse inoculated with the E-330V/NS1-98W virus. The eye, testis, seminal vesicle, and vas deferens showed no histopathologic changes and no viral RNA labeling by ISH for mice inoculated with E-330L/NS1-98W and E-330L/NS1-98G viruses, except for one focal region of seminal vesicle mucosal staining by ISH in one mouse inoculated with the E-330L/NS1-98G virus.

Epididymides had epithelial necrosis and subacute inflammation with ZIKV RNA localization to luminal sloughed cells and epididymal epithelium in all groups. These findings were generally more prominent in epididymal heads, decreasing distally with relative sparing of epididymal tails, where only scattered tubules were affected. However, for the one mouse inoculated with the E-330V/NS1-98W virus that did not have a testicular teratoma, inflammatory and degenerative changes extended more diffusely throughout the epididymis, and there was extensive ZIKV RNA localization within luminal and epithelial cells throughout the body and tail of the epididymis (Fig. 5B, fifth panel). The two mice with testicular teratomas lacked intraluminal spermatozoa and had comparatively rare staining by ISH.

2.4. Increased fitness of E-V330L/NS1-W98G in Vero cells

Given that the E-330L and NS1-98G variants arose within three passages of the PRVABC59 isolate in Vero cells, the viruses containing these mutations were evaluated for relative growth capacities in Vero cells. The E-330L/NS1-98G virus reached higher titers in Vero cells than the E-330V/NS1-98W or the E-330L/NS1-98W viruses (Fig. 6A, $p < 0.0001$). To determine whether the NS1-98G mutation indeed conferred a fitness advantage, an *in vitro* competition study was performed. The E-330V/NS1-98W virus was mixed with the E-330L/NS1-98W or the E-330L/NS1-98G viruses at a ratio of 10:1 and passaged in triplicate in Vero cells three times. In the E-330V/NS1-98W: E-330L/NS1-98W competition, both viruses remained present at a stable ratio throughout passaging (Fig. 6B, left panel). However, in the E-330V/NS1-98W: E-330L/NS1-98G competition, the E-330L/NS1-98G virus increased in proportion over the three passages (Fig. 6B, right panel). These data indicate that incorporation of the E-V330L and NS1-W98G mutations resulted in elevated fitness in Vero cells.

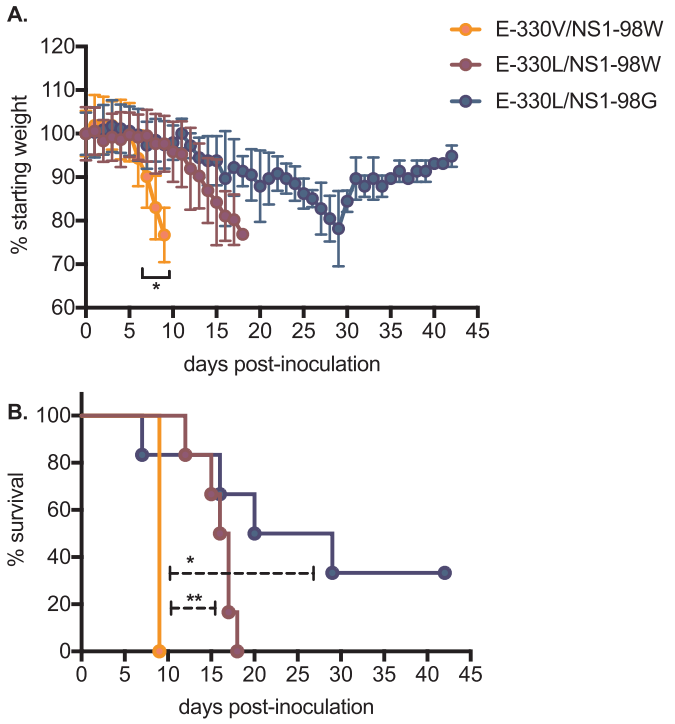

Fig. 2. Morbidity and mortality of ZIKV mutants in AG129 mice. Yellow symbols represent mice inoculated with ZIKV E-330V/NS1-98W (n = 12); red symbols represent mice inoculated with ZIKV E-330L/NS1-98W (n = 12); and blue symbols represent mice inoculated with ZIKV E-330L/NS1–98 G (n = 12). Three mice from each group were sacrificed on dpi 6 and dpi 9, such that time points after dpi 6 and 9 are representative of n = 9 or 6 mice, respectively. (A) Average weight of mice post-inoculation, represented as a percentage of initial weight. Error bars represent standard deviations. (B) Daily percent survival of mice post-inoculation. Error bars represent standard deviations. * $p < 0.05$, * * $p < 0.001$.

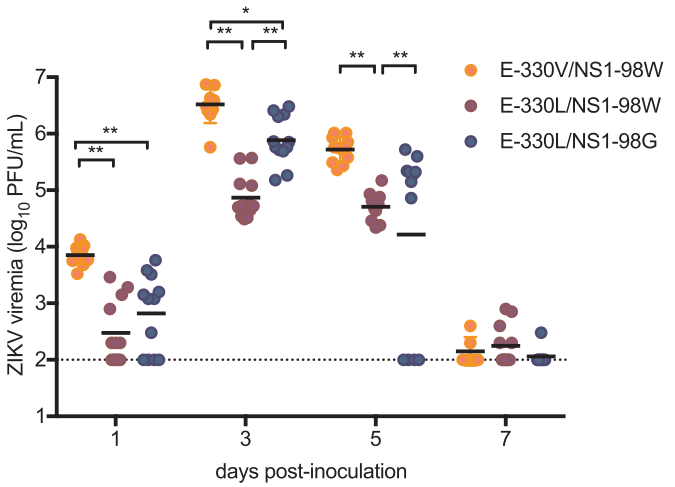

Fig. 3. Viremia of ZIKV mutants in mice. Yellow symbols represent mice inoculated with ZIKV E-330V/NS1-98W (n = 12); red symbols represent mice inoculated with ZIKV E-330L/NS1-98W (n = 12); and blue symbols represent mice inoculated with ZIKV E-330L/NS1-98 G (n = 12). Three mice from each group were sacrificed on dpi 6, such that time points after dpi 6 are representative of n = 9 mice. Mean viremia (PFU/mL sera) of mice. * $p < 0.05$, * * $p < 0.001$.

3. Discussion

Two non-synonymous variants at residues E-330 and NS1–98 were identified in the ZIKV isolate PRVABC59 when the sequence of the original patient sera sample was compared to the widely-distributed Vero passage three isolate. Following inoculation of male AG129 mice with the passage three PRVABC59 isolate, these variants increased further in frequency, suggesting selection in mice. However, mice subsequently inoculated with viruses containing the derived ZIKV E-330L mutation, with or without the NS1-98G mutation, experienced delayed mortality and decreased viral dissemination to the eye and brain compared to the original E-330V/NS1-98W virus, indicating these variants are attenuating in mice. Yet, viruses containing the E-330L/NS1-98G mutations were more fit in Vero cell culture. These results, coupled with the very low frequencies of these variants in the initial patient serum, suggest the variants arose during initial passaging of the isolate, perhaps due to increased fitness in Vero cells conferred by the mutations. Furthermore, these results indicate that the E-330 locus is a determinant of ZIKV pathogenesis in mice.

Cell culture adaptive mutations in flaviviruses have been described previously (Puig-Basagoiti et al., 2007; Ciota et al., 2007). The E-V330L/NS1-W98G mutations may increase fitness in Vero cells by causing an increase in binding and uptake in cultured cells. While not specifically shown in this study to independently modulate Vero growth fitness, the E-V330L mutation could epistatically augment Vero cell fitness with NS1-W98G, another protein that, although not expressed on the surface of the virion, is secreted from infected cells. Both envelope and NS1 can bind glycosaminoglycans (GAGs) on the plasma membrane of the cell (Avirutnan et al., 2007). Viral adaptation to cell culture systems can result in envelope modifications to optimize binding to GAGs that facilitate viral entry but that concomitantly result in reduced levels of circulating virus and subsequently reduced *in vivo* virulence. This has been described extensively for alphaviruses that commonly incorporate positively charged residues on their surface envelope domains to more efficiently bind negatively charged GAGs (Wang et al., 2003; Klimstra et al., 1998). Additionally, flaviviruses such as Japanese encephalitis virus (Lee et al., 2004), tick-borne encephalitis virus (Kozlovskaya et al., 2010) and the 17D yellow fever live viral vaccine have demonstrated GAG binding that has been accentuated by cell culture passage. Increased GAG binging of 17D compared to wildtype virus has specifically been implicated with reduced viscerotropism/attenuation of 17D (Lee and Lobigs, 2008). A specific E-T380R mutation, found in all 17D sub-strains and that encodes a positive charge modification, results in enhanced GAG binding and loss of virulence. Dengue virus culture passage mutations have also specifically been associated with increased GAG binding efficiency and reduced neuroinvasiveness (Lee et al., 2006). However, in this case, it is unclear whether the same mechanism is involved, as the valine to leucine change at E-330 would not alter charge.

In agreement with these previous studies, the E-V330L mutation conferred a decreased neuroinvasive phenotype in AG129 mice but did not negatively impact the dissemination to the epididymis by day 9. This could explain the frequency of these variants in the reproductive tract and seminal fluids of male mice infected with the Vero passage three isolate. Unfortunately, the high virulence of the mutant containing E-330V precluded a direct assessment of the role of this mutation on seminal transmission efficiency in the AG129 males. Viral infection in the epididymis and specifically within the epididymal tail has previously been associated with sexual transmission potential in this mouse model (McDonald et al., 2018). Thus, although testes titers were higher for the E-330V/NS1-98W virus compared to the E-330L/NS1-98G virus, the indistinguishable levels of virus in the epididymis of mice inoculated with these viruses indicates that altered sexual transmissibility would be unlikely.

Many studies have found decreased pathogenicity of the Asian genotype ZIKV isolates compared to the African genotype ZIKV isolates in mice (McDonald et al., 2017; Smith et al., 2018), as well as low *in utero* transmission rates and mosquito infection from infected non-human primates (Aliota et al., 2018; Dudley et al., 2017). This may be partially due to the attenuation of PRVABC59 that occurred with as few

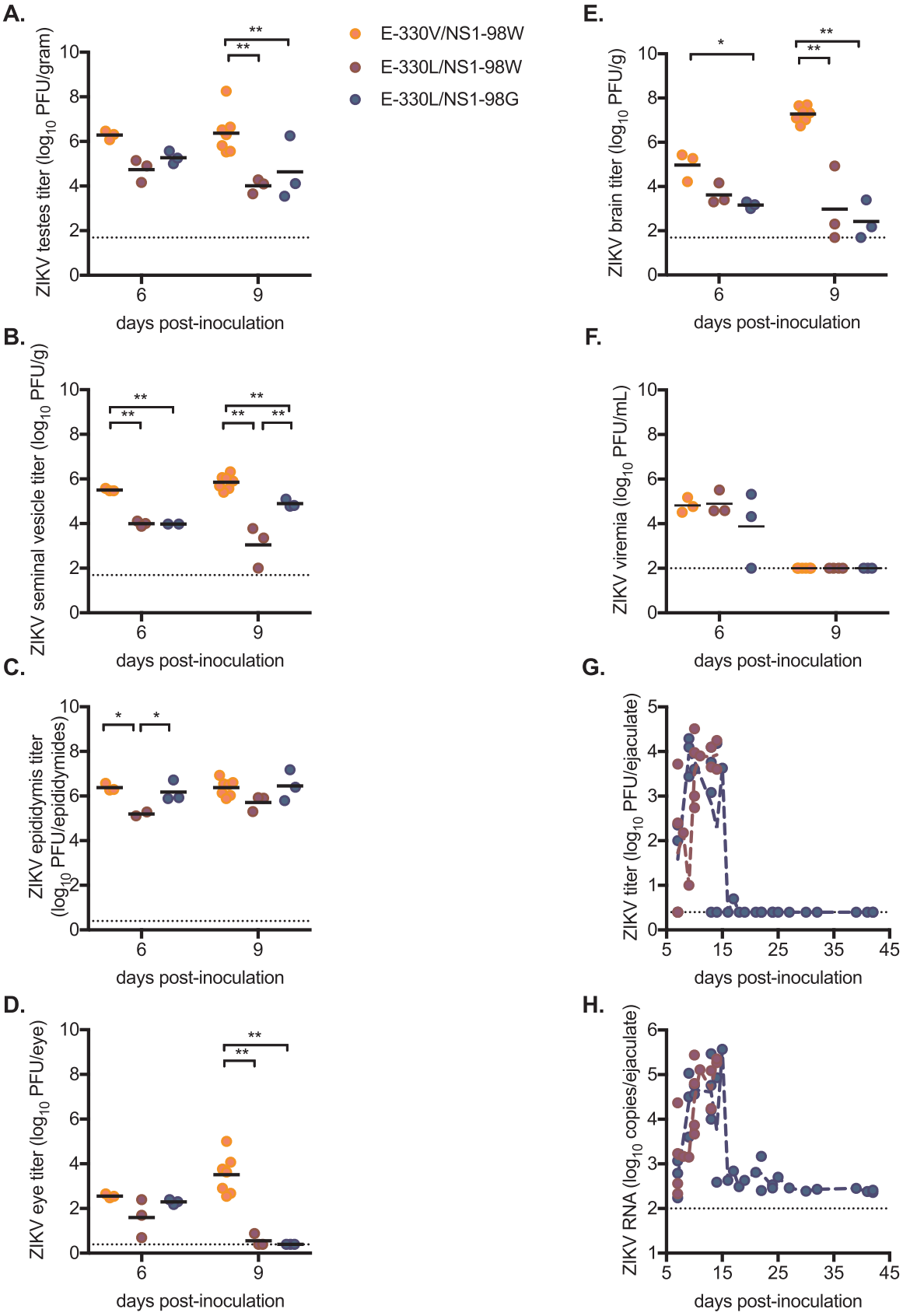

Fig. 4. Viral titers of ZIKV mutants in mouse tissues. Yellow symbols represent mice inoculated with ZIKV E-330V/NS1-98W (n = 3); red symbols represent mice inoculated with ZIKV E-330L/NS1-98W (n = 3); and blue symbols represent mice inoculated with ZIKV E-330L/NS1-98 G (n = 3). Titers from tissues, sera, and ejaculates are represented as PFU per gram of tissue, per of mL sera, and per ejaculate, respectively. Titers from individual mice are represented by circles, with means represented by solid lines. The limit of detection is represented by a dashed gray line. ZIKV titer in (A) testes; (B) seminal vesicles; (C) epididymides; (D) eye; (E) brain; (F) serum; (G) ejaculates; and (H) ejaculates (log_{10} RNA copies/ejaculate) *$p < 0.05$, * *$p < 0.001$, * * * $p < 0.0001$.

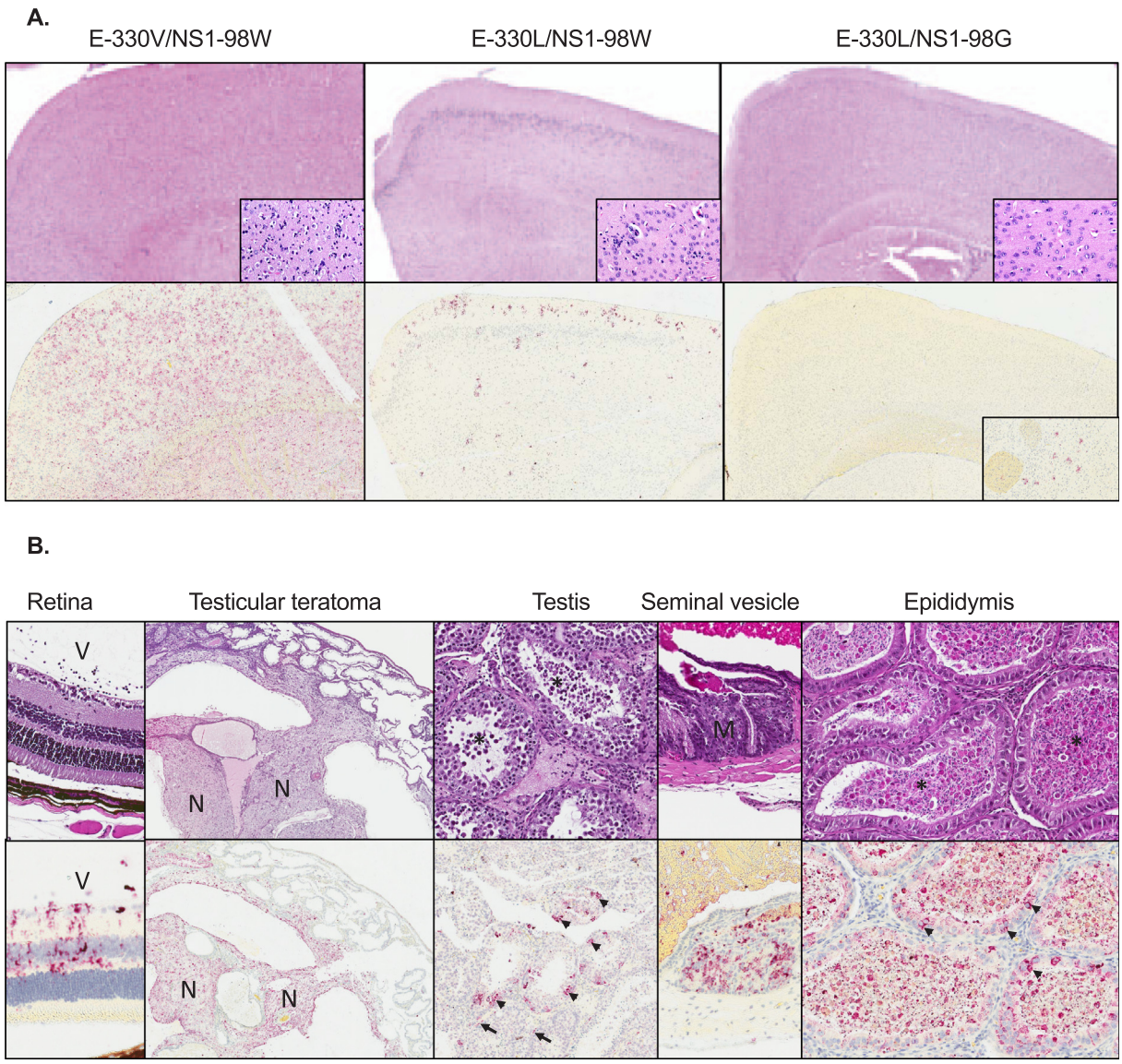

Fig. 5. Pathology and ZIKV ISH in mouse tissues. Tissues were stained with H&E (top) or by ISH for ZIKV RNA (bottom). (A) Parasagittal sections of cerebrum from mice inoculated with ZIKV E-330V/NS1-98W (left), E-330L/NS1-98W (middle), or E-330L/NS1-98G (right). Original magnifications: 40 × (H&E and ISH), 400 × (H&E insets), 80 × (ISH inset). (B) Eye, testis, and seminal vesicle from mice inoculated with E-330V/NS1-98W. The vitreous chamber (V) of the eye, neural component (N) of the testes, and mucosal necrosis (M) in the seminal vesicle are marked. In the testis, ZIKV ISH staining of scattered epithelial cells and peritubular myoid cells (arrowheads) are indicated. In the epididymides, sperm (*) and ZIKV ISH straining of lining epithelium (arrowheads) are indicated. Original magnifications: 200 × (retina, testis H&E, seminal vesicle, epididymis), 40 × (teratoma), 100 × (testis ISH).

as three passages in cell culture. However, sequences for other ZIKV isolates do not display a leucine at E-330, suggesting this attenuation may be specific to PRVABC59. Future animal experiments should consider use of the clone-derived ZIKV with a valine at E-330 to reduce the potential contribution of cell culture derived mutations to pathogenesis and/or vaccine efficacy studies.

4. Materials and methods

4.1. Deep sequencing of ZIKV

Unbiased library prep was performed similarly to (Matranga et al., 2014). Briefly, viral RNA was extracted from PRVABC59 passage 3 stocks in duplicate using the MagMax 96 Viral RNA kit (Ambion). rRNA was depleted using the RNase H selective depletion method with modifications using in-house probes targeting mouse rRNA. Briefly, AMV reverse transcriptase (NEB) was added with probes, DNA:RNA hybrids were degraded with RNase H (NEB), and probes were degraded with DNase I (Promega). RNA was purified using AMpure RNAclean beads (Beckman Coulter). Double-stranded cDNA was generated using random primers, Superscript IV RT (Invitrogen), and NEBNext Ultra II Q5 polymerase, and fragmented using Nextera XT (Illumina). Illumina adapters were added by 12 cycles of PCR using Q5 polymerase and purified with AMpure XP beads (Beckman Coulter). Libraries were amplified using a Kapa real-time library amplification kit and size-selected using AMpure XP beads. Libraries were quantified with a NEB library quantification kit, and fragment sizes were measured by Tapestation (Agilent). Libraries were pooled equally and sequenced on an Illumina Nextseq with 300 bp paired-end reads.

Reads were demultiplexed using Bcl2fastq and trimmed for adapters and low quality using BBDuk (part of the BBTools suite, https://sourceforge.net/projects/bbmap/). BBMap was used to align the trimmed reads to the PRVABC59 reference sequence and variants were called using LoFreq. 2.1 (Wilm et al., 2012).

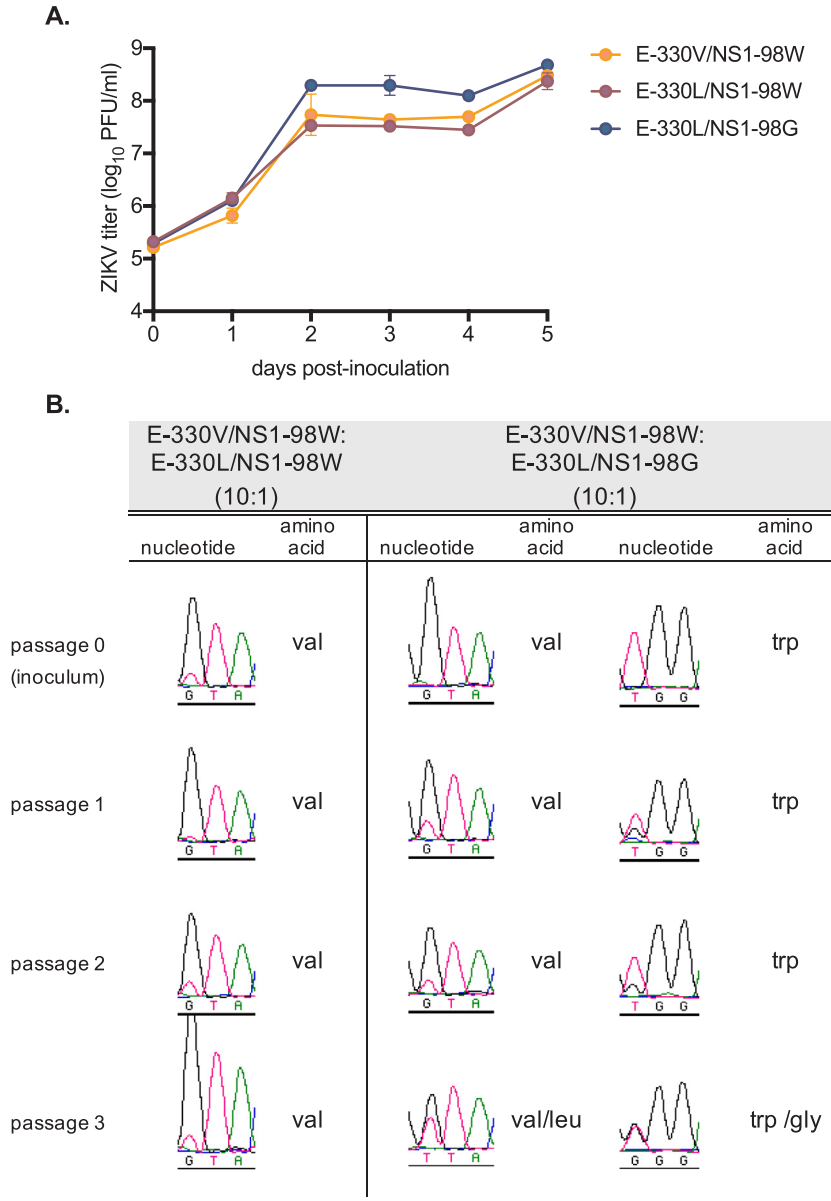

Fig. 6. Adaptation of ZIKV mutants to Vero cells. (A) Growth curve of ZIKV mutants in Vero cells. Symbols represent the average titer of triplicate wells inoculated with the ZIKV E-330V/NS1-98W (yellow); ZIKV E-330L/NS1-98W virus (red); and ZIKV E-330L/NS1-98G virus (blue). Error bars represent standard deviations. Growth curves were performed twice, and one representative experiment is shown. (B) *in vitro* competition experiment. Chromatograms from passage 0 (inoculum) through passage 3 are show. The experiment was performed in triplicate, and one representative replicate is shown.

4.2. Mutagenesis of ZIKV infectious clone

The two-part ZIKV PRVABC59 infectious clone system that we have previously described was used to make all mutations (Weger-Lucarelli et al., 2017). Plasmid mutagenesis was performed using IVA cloning (Garcia-Nafria et al., 2016) following the protocol with the exception that Q5 polymerase was used instead of Phusion. Primer sequences are available upon request. Viruses were rescued as described in (Weger-Lucarelli et al., 2017) and sequenced to confirm identity.

4.3. Mouse inoculations

Mice deficient in interferon α/β and -γ receptors (AG129 mice) were bred in-house, and the receptor knockout genotype of the mice was confirmed as described previously (Duggal et al., 2017a). Thirty-six 12–16-week-old male mice were inoculated subcutaneously in the rear footpad with 3 $\log_{10}$ PFU of ZIKV strains E-330L/NS1-98G, E-330L/NS1-98W or E-330V/NS1-98W diluted in PBS. Mice were weighed daily and checked twice a day for signs of morbidity. Serial blood samples were obtained on dpi 1, 3, 5 and 7 from the submandibular vein. Mice were euthanized after isoflurane-induced deep anesthesia followed by cervical dislocation. Tissues were collected at time of euthanasia. For plaque assays, brain, testes, and seminal vesicles were weighed and re-suspended in an equal volume of BA-1 medium. The eye was re-suspended in 25 µL of BA-1 medium. These tissues were then homogenized using a pestle. All tissues were clarified by centrifugation and serially diluted for cell plaque assay to enumerate plaque forming units (PFU).

4.4. Collection of seminal fluids from male AG129 mice

Seminal fluids from male AG129 mice were collected as previously described (Duggal et al., 2017a). In brief, inoculated male mice were housed individually, and each evening beginning on dpi 7 three female CD-1 mice were introduced into the cage. The following morning,

mating activity was determined by the presence of a copulatory plug in the female. Mated females were euthanized by isoflurane anesthesia followed by cervical dislocation. 500 µL of BA-1 media was used to gavage both horns of the uterus. Infectious ZIKV in the seminal fluids was titrated by Vero cell plaque assay, and RNA was quantified by real-time RT-PCR as described previously (Duggal et al., 2017a).

4.5. Tissue histology and RNA in situ hybridization

Tissues were fixed in 10% neutral buffered formalin for 3 days and then stored in 70% ethanol prior to routine processing and paraffin-embedding. Sections were cut at 4 µm and stained by H&E for histopathological evaluation, or by *in situ* hybridization (ISH) as previously described (Duggal et al., 2018).

4.6. In vitro growth curve

Vero cells were grown at 37 °C with 5% CO2 in DMEM supplemented with 10% FBS and 1% penicillin-streptomycin. Cells were plated at 1.5×10^5 cells/well in 12-well plates and inoculated when 80% confluent at an MOI of 0.1. Timepoints were taken daily and titrated by Vero cell plaque assay.

4.7. Competition assay

Vero cells were plated at 1.5×10^5 cells/well in 12-well plates. At 80% confluency, cells were inoculated with a 1:10 mix of viruses at an MOI of 0.1 in triplicate. Viruses were harvested on dpi 2 and titrated by Vero plaque assay. The virus was then passaged again in triplicate at an MOI of 0.1 for a total of 3 passages. Viral RNA was extracted from all samples using Quick-RNA Viral Kit (Zymo) and amplified using OneStep RT-PCR (Qiagen) using primers 1711F (5′- CAAGGACGCACA TGCCAAAA-3′) and 2964 R (5′- TACCCCGAACCCATGATCCT-3′). Amplicons sequenced directly by Sanger sequencing. Chromatograms were viewed in DNAstar v14.

4.8. Statistics

Survival curves were compared using a Log-Rank (Mantel Cox) test. Mean weights and viral titers were compared using ANOVA. Statistics were performed in GraphPad Prism 7.

Acknowledgements

This work was supported in part by NIH grant AI067380 (G.D.E.). We thank DVBD staff members Jason Velez for cell culture support and Sean Masters for his excellent contributions to animal husbandry and animal care needs throughout this study. The findings and conclusions of this report are those of the authors and do not necessarily represent the official position of the Centers for Disease Control and Prevention or the U.S. Agency for International Development.

References

Aliota, M.T., Dudley, D.M., Newman, C.M., Weger-Lucarelli, J., Stewart, L.M., Koenig, M.R., et al., 2018. Molecularly barcoded Zika virus libraries to probe in vivo evolutionary dynamics. PLoS Pathog. 14 (3), e1006964. https://doi.org/10.1371/journal.ppat.1006964.

Avirutnan, P., Zhang, L., Punyadee, N., Manuyakorn, A., Puttikhunt, C., Kasinrerk, W., et al., 2007. Secreted NS1 of dengue virus attaches to the surface of cells via interactions with heparan sulfate and chondroitin sulfate E. PLoS Pathog. 3 (11), e183. https://doi.org/10.1371/journal.ppat.0030183.

Ciota, A.T., Lovelace, A.O., Ngo, K.A., Le, A.N., Maffei, J.G., Franke, M.A., et al., 2007. Cell-specific adaptation of two flaviviruses following serial passage in mosquito cell culture. Virology 357 (2), 165–174. https://doi.org/10.1016/j.virol.2006.08.005.

Dudley, D.M., Newman, C.M., Lalli, J., Stewart, L.M., Koenig, M.R., Weiler, A.M., et al., 2017. Infection via mosquito bite alters Zika virus tissue tropism and replication kinetics in rhesus macaques. Nat. Commun. 8 (1), 2096. https://doi.org/10.1038/s41467-017-02222-8.

Duggal, N.K., Ritter, J.M., Pestorius, S.E., Zaki, S.R., Davis, B.S., Chang, G.J., et al., 2017a. Frequent Zika virus sexual transmission and prolonged viral RNA shedding in an immunodeficient mouse model. Cell Rep. 18 (7), 1751–1760. https://doi.org/10.1016/j.celrep.2017.01.056.

Duggal, N.K., Ritter, J.M., McDonald, E.M., Romo, H., Guirakhoo, F., Davis, B.S., et al., 2017b. Differential neurovirulence of African and Asian genotype Zika virus isolates in outbred immunocompetent mice. Am. J. Trop. Med. Hyg. https://doi.org/10.4269/ajtmh.17-0263.

Duggal, N.K., McDonald, E.M., Ritter, J.M., Brault, A.C., 2018. Sexual transmission of Zika virus enhances in utero transmission in a mouse model. Sci. Rep. 8 (1), 4510. https://doi.org/10.1038/s41598-018-22840-6.

Garcia-Nafria, J., Watson, J.F., Greger, I.H., 2016. IVA cloning: a single-tube universal cloning system exploiting bacterial in vivo assembly. Sci. Rep. 6, 27459. https://doi.org/10.1038/srep27459.

Govero, J., Esakky, P., Scheaffer, S.M., Fernandez, E., Drury, A., Platt, D.J., et al., 2016. Zika virus infection damages the testes in mice. Nature. https://doi.org/10.1038/nature20556.

Joseph, S.B., Swanstrom, R., Kashuba, A.D., Cohen, M.S., 2015. Bottlenecks in HIV-1 transmission: insights from the study of founder viruses. Nat. Rev. Microbiol. 13 (7), 414–425. https://doi.org/10.1038/nrmicro3471.

Klimstra, W.B., Ryman, K.D., Johnston, R.E., 1998. Adaptation of Sindbis virus to BHK cells selects for use of heparan sulfate as an attachment receptor. J. Virol. 72 (9), 7357–7366.

Kozlovskaya, L.I., Osolodkin, D.I., Shevtsova, A.S., Romanova, L., Rogova, Y.V., Dzhivanian, T.I., et al., 2010. GAG-binding variants of tick-borne encephalitis virus. Virology 398 (2), 262–272.

Lanciotti, R.S., Lambert, A.J., Holodniy, M., Saavedra, S., Signor Ldel, C., 2016. Phylogeny of Zika virus in Western hemisphere, 2015. Emerg. Infect. Dis. 22 (5), 933–935. https://doi.org/10.3201/eid2205.160065.

Lazear, H.M., Govero, J., Smith, A.M., Platt, D.J., Fernandez, E., Miner, J.J., et al., 2016. A mouse model of Zika virus pathogenesis. Cell Host Microbe 19 (5), 720–730. https://doi.org/10.1016/j.chom.2016.03.010.

Lee, E., Lobigs, M., 2008. E protein domain III determinants of yellow fever virus 17D vaccine strain enhance binding to glycosaminoglycans, impedes virus spread and attenuates virulence. J. Virol.

Lee, E., Hall, R.A., Lobigs, M., 2004. Common E protein determinants for attenuation of glycosaminoglycan-binding variants of Japanese encephalitis and West Nile viruses. J. Virol. 78 (15), 8271–8280. https://doi.org/10.1128/JVI.78.15.8271-8280.2004.

Lee, E., Wright, P.J., Davidson, A., Lobigs, M., 2006. Virulence attenuation of Dengue virus due to augmented glycosaminoglycan-binding affinity and restriction in extraneural dissemination. J. Gen. Virol. 87 (Pt 10), 2791–2801.

Ma, W., Li, S., Ma, S., Jia, L., Zhang, F., Zhang, Y., et al., 2016. Zika virus causes testis damage and leads to male infertility in mice. Cell 167 (6), 1511–24 e10. https://doi.org/10.1016/j.cell.2016.11.016.

Matranga, C.B., Andersen, K.G., Winnicki, S., Busby, M., Gladden, A.D., Tewhey, R., et al., 2014. Enhanced methods for unbiased deep sequencing of Lassa and Ebola RNA viruses from clinical and biological samples. Genome Biol. 15 (11), 519. https://doi.org/10.1186/PREACCEPT-1698056557139770.

McDonald, E.M., Duggal, N.K., Brault, A.C., 2017. Pathogenesis and sexual transmission of Spondweni and Zika viruses. PLoS Negl. Trop. Dis. 11 (10), e0005990. https://doi.org/10.1371/journal.pntd.0005990.

McDonald, E.M., Duggal, N.K., Ritter, J.M., Brault, A.C., 2018. Infection of epididymal epithelial cells and leukocytes drives seminal shedding of Zika virus in a mouse model. PLoS Negl. Trop. Dis. 12 (8), e0006691. https://doi.org/10.1371/journal.pntd.0006691.

Puig-Basagoiti, F., Tilgner, M., Bennett, C.J., Zhou, Y., Munoz-Jordan, J.L., Garcia-Sastre, A., et al., 2007. A mouse cell-adapted NS4B mutation attenuates West Nile virus RNA synthesis. Virology 361 (1), 229–241. https://doi.org/10.1016/j.virol.2006.11.012.

Rossi, S.L., Tesh, R.B., Azar, S.R., Muruato, A.E., Hanley, K.A., Auguste, A.J., et al., 2016. Characterization of a novel Murine model to study Zika virus. Am. J. Trop. Med. Hyg. 94 (6), 1362–1369. https://doi.org/10.4269/ajtmh.16-0111.

Smith, D.R., Sprague, T.R., Hollidge, B.S., Valdez, S.M., Padilla, S.L., Bellanca, S.A., et al., 2018. African and Asian Zika virus isolates display phenotypic differences both In vitro and In vivo. Am. J. Trop. Med. Hyg. 98 (2), 432–444. https://doi.org/10.4269/ajtmh.17-0685.

Wang, E., Brault, A.C., Powers, A.M., Kang, W., Weaver, S.C., 2003. Glycosaminoglycan binding properties of natural Venezuelan equine encephalitis virus isolates. J. Virol. 77 (2), 1204–1210.

Weger-Lucarelli, J., Duggal, N.K., Bullard-Feibelman, K., Veselinovic, M., Romo, H., Nguyen, C., et al., 2017. Development and characterization of recombinant virus generated from a new world Zika virus infectious clone. J. Virol. 91 (1). https://doi.org/10.1128/JVI.01765-16.

Wilm, A., Aw, P.P., Bertrand, D., Yeo, G.H., Ong, S.H., Wong, C.H., et al., 2012. LoFreq: a sequence-quality aware, ultra-sensitive variant caller for uncovering cell-population heterogeneity from high-throughput sequencing datasets. Nucleic Acids Res. 40 (22), 11189–11201. https://doi.org/10.1093/nar/gks918.